Quantification of the discontinuity of the temperature variance dissipation rate: wall-resolved LES of turbulent channel flow with conjugate heat transfer

Cédric Flageul, Iztok Tiselj, Sofiane Benhamadouche, Martin Ferrand

QUANTIFICATION OF THE DISCONTINUITY OF THE TEMPERATURE VARIANCE DISSIPATION RATE: WALL-RESOLVED LES OF TURBULENT CHANNEL FLOW WITH CONJUGATE HEAT TRANSFER

C. Flageul and I. Tiselj
Reactor Engineering Division
Institute Jožef Stefan, Ljubljana, Slovenia
cedric.flageul@ijs.si; iztok.tiselj@ijs.si

S. Benhamadouche and M. Ferrand
Fluid Mechanics Energy and Environment Dept.
EDF R&D, Chatou, France
sofiane.benhamadouche@edf.fr; martin.ferrand@edf.fr

ABSTRACT

Conjugate heat transfer represents the actual thermal coupling between a fluid and a solid part. It is of prime importance in nuclear industrial applications where fluctuating thermal stresses are a concern, e.g. in case of a severe emergency cooling (Pressurized Thermal Shock) or long-term ageing of materials such as thermal striping occurring in T-junctions. For such complex applications, numerical investigations often rely on Reynolds Averaged Navier Stokes (RANS) or wall-modelled Large Eddy Simulation (LES) approaches. RANS models for conjugate heat transfer are relatively recent (Craft et al., [1]). Using Direct Numerical Simulation (DNS), the authors and coworkers have recently established that the dissipation rate (ε_θ) associated with the halved temperature variance ($\theta'^2/2$) is discontinuous at the fluid-solid interface in case of conjugate heat transfer (Flageul et al., [2-3]). Actually, there is currently no coupled RANS model for conjugate heat transfer taking this discontinuity into account. As a result, from an industrial perspective, LES remains the best option for thermal fatigue prediction but needs refinement at the wall, which makes it very expensive if not unaffordable, at high Reynolds numbers. In this paper, we will assess the ability of wall-resolved LES to estimate this discontinuity of ε_θ on channel flows ($Re = 7060, Pr = 0.71$) using *Code_Saturne*, EDF in-house and open-source CFD software.

KEYWORDS
Conjugate heat transfer, wall-resolved LES, Temperature variance dissipation rate

1. INTRODUCTION

Conjugate heat transfer describes the thermal coupling between a fluid and a solid. It is of prime importance in industrial applications where fluctuating thermal stresses are a concern. As far as the nuclear industry is concerned, relevant applications include severe emergency cooling (Pressurized Thermal Shock) or long-term ageing of materials (T junctions). For such complex applications, characterized by high Reynolds number, investigations often rely on experiments, high Reynolds RANS or wall-modelled LES. However, experimental data on conjugate heat transfer are scarce as walls in lab rigs are often made of plexiglas and the transported scalar studied is often a dye. The development of RANS models for conjugate heat transfer is relatively recent (Craft et al., [1]).

In [2-3], the authors have established that in case of conjugate heat-transfer, the dissipation rate (ε_θ) associated with the halved variance of the temperature ($\theta'^2/2$) is discontinuous at the fluid-solid interface; thus, challenging the ability of (U)RANS models to investigate configurations with conjugate heat-transfer. As a result, from an industrial perspective, LES remains the best option for thermal fatigue prediction but needs refinement at the wall, which makes it very expensive if not unaffordable, at high Reynolds numbers.

Experimental data on conjugate heat transfer are scarce, expensive and difficult to carry out in order to obtain fine quantities such as ε_θ. This makes DNS and wall-resolved LES the only solutions to obtain such data. In this paper, in order to deal with higher Reynolds numbers than in DNS, we will assess the ability of wall-resolved Large Eddy Simulation to estimate this discontinuity of ε_θ on channel flows using *Code_Saturne*, EDF in-house and open-source CFD software. This is a step forward towards a rich validation database for future RANS models adapted to conjugate heat transfer.

The structure of this paper is as follows. In the second section, governing equations are presented alongside with their numerical discretization. In the third section, the cases simulated are fully described. In the fourth section, the results are presented. In the fifth section, they are further discussed alongside with their consequences for RANS and LES modeling.

2. GOVERNING EQUATIONS AND DISCRETIZATION

The equations presented hereafter assume that the fluid is Newtonian with constant physical properties and that the flow is incompressible. They also assume that the thermal properties in the solid domain are constant, although they may differ from the fluid ones. Naturally, the discontinuity of ε_θ at the fluid-solid interface holds for compressible flows or when physical properties are variable.

2.1. Governing Equations

The continuity equation reads:

$$\partial_k U_k = 0 \tag{1}$$

The momentum equation for direction i reads:

$$\partial_t U_i = -U_j \partial_j (U_i) - \partial_i p + \partial_j \left[(\nu + \nu_t) S_{ij} \right] + f_i \text{ with } 2S_{ij} = \partial_j U_i + \partial_i U_j \tag{2}$$

The source term f_i is a constant pressure gradient and is active only in the streamwise direction. When using the WALE model, the subgrid-scale (SGS) turbulent viscosity ν_t is defined by:

$$\nu_t = 4\sqrt{2}(V_{cell})^{2/3}(C_w)^2 \frac{\left(S_{ij}^d S_{ij}^d\right)^{3/2}}{\left(S_{ij}S_{ij}\right)^{5/2} + \left(S_{ij}^d S_{ij}^d\right)^{5/4}} \text{ with } C_w = 0.25 \tag{3}$$

In equation (3), S_{ij}^d is the traceless symmetric part of the square of the velocity gradient tensor, as defined by Nicoud and Ducros, [4]. In case of conjugate heat transfer, the energy equation reads:

$$\partial_t T_f = -U_j \partial_j (T_f) + \partial_j \left[\left(\alpha_f + \frac{\nu_t}{Pr_t} \right) \partial_j (T_f) \right] + f_T \text{ in the fluid domain } \Omega_f. \tag{4}$$

$$\partial_t T_s = \partial_j \left[\alpha_s \partial_j (T_s) \right] \text{ in the solid domain } \Omega_s. \tag{5}$$

$$T_f = T_s \text{ and } \lambda_f \partial_n T_f = \lambda_s \partial_n T_s \text{ at the fluid-solid interface } \partial\Omega_f \cap \partial\Omega_s. \quad (6)$$

In equation (4), the turbulent Prandtl number Pr_t, is set to 0.5 (Grötzbach [5]) and the source term f_T is as defined by Kasagi et al., [6]. In equation (6), ∂_n is the derivative along the vector normal to the fluid-solid interface. This equation is a direct transcription of the continuity of the temperature and heat-flux across the interface.

Following Tiselj and Cizelj, [7], 2 independent dimensionless numbers describe this fluid-solid thermal coupling:

$$G = \frac{\alpha_f}{\alpha_s} \text{ and } K = \frac{\lambda_f}{\lambda_s \sqrt{G}} \quad (7)$$

In equation (7), G is the fluid-to-solid thermal diffusivity ratio and K is the thermal activity ratio, which is also the fluid-to-solid thermal effusivity ratio. The thermal properties ratios (alongside with the Reynolds and Prandtl number) used in our simulations are further described in section 3.

Following Flageul et al., [2-3], in case of conjugate heat transfer, ε_θ is discontinuous at the fluid-solid interface and satisfies:

$$\frac{\varepsilon_{\theta,s}}{\varepsilon_{\theta,f}} = \frac{\overline{\partial_n T_f' \partial_n T_f'}}{\overline{\partial_\iota T_f' \partial_\iota T_f'}} K^2 + \left(1 - \frac{\overline{\partial_n T_f' \partial_n T_f'}}{\overline{\partial_\iota T_f' \partial_\iota T_f'}}\right) \frac{1}{G} \text{ at the fluid-solid interface } \partial\Omega_f \cap \partial\Omega_s. \quad (8)$$

As equation (8) is a convex combination, the ratio of the solid-to-fluid dissipation rates at the fluid-solid interface is bounded by K^2 and $1/G$. Equation (8) holds as long as the vector normal to the fluid-solid interface is well-defined, which means any flat or curved interface. It becomes ill-defined only at edges or corners.

In [2-3], equation (8) was derived in the absence of SGS model ($\nu_t = 0$) using dissipation rates defined by:

$$\varepsilon_{\theta,f} = \alpha_f \overline{\partial_\iota T_f' \partial_\iota T_f'} \text{ and } \varepsilon_{\theta,s} = \alpha_s \overline{\partial_\iota T_s' \partial_\iota T_s'} \quad (9)$$

In this paper, we will examine the validity of equation (8) for wall-resolved LES of the turbulent channel flow using the WALE model, a constant turbulent Prandtl number of 0.5 and dissipation rates defined by:

$$\varepsilon_{\theta,f} = \overline{\left(\alpha_f + \frac{\nu_t}{Pr_t}\right) \partial_\iota T_f' \partial_\iota T_f'} \text{ and } \varepsilon_{\theta,s} = \alpha_s \overline{\partial_\iota T_s' \partial_\iota T_s'} \quad (10)$$

ε, the dissipation rate of the turbulent kinetic energy is similarly defined by:

$$\varepsilon = \overline{(\nu + \nu_t) \partial_\iota u_j' \partial_\iota u_j'} \quad (11)$$

2.2. Discretization

Our LES are performed with the open source solver *Code_Saturne* (www.code-saturne.org), an unstructured collocated finite volume solver for incompressible flows. It uses a SIMPLEC algorithm for pressure-velocity coupling, which requires Rhie and Chow interpolation to avoid odd-even oscillations.

Since version 5.0, *Code_Saturne* can be used stand-alone to perform conjugate heat-transfer with simultaneous solving of the fluid and solid temperature.

As our meshes are made of orthogonal hexahedra, no gradient reconstruction sweeps are needed. In addition, the existing slope-test by default is deactivated for the scalars. As a result, for the velocity and the temperature, a fully centered scheme is used, combined with a Crank-Nicolson time scheme. The convective term is linearized and the transporting velocity uses an Adams-Bashforth time scheme. Further details about *Code_Saturne* can be found in Archambeau et al., [8].

3. CASE SETUP

The structure of this section is as follows. In the first subsection, the validation case is presented. It corresponds to a Reynolds number of 2280 based on the bulk velocity (150 based on the friction velocity) and uses DNS data from Flageul et al. [2-3]. In the second subsection, 2 other cases are described. They both correspond to a Reynolds number of 7060 based on the bulk velocity (395 based on the friction velocity) but the thickness of the solid part differs.

In the present study, x, y and z stand for the streamwise, wall-normal and spanwise directions, respectively. Periodic boundary conditions are used in the directions x and z. For all the configurations, the extension of the solid domain in the directions x and z is identical to the fluid one.

All the DNS and LES are performed with a Prandtl number ($Pr = \nu/\alpha_f$) of 0.71. The Reynolds number (Re) based on the bulk velocity is defined with the kinematic viscosity ν, the channel half-height and the averaged bulk velocity, the two latter equaling unity in the present study. For cases with conjugate heat transfer, an imposed heat flux is always used at the outer wall.

For each case, 2 LES are performed: one without SGS model ($\nu_t = 0$) and one with the WALE model combined with a constant turbulent Prandtl number (Pr_t) of 0.5.

3.1. Validation Case at Re=2280

For the validation case at Re=2280, Table I summarizes the simulation parameters.

Table I. Simulation parameters for the case Re=2280

	Present	**Flageul et al. [2-3]**
Fluid domain extension	[12.56, 2, 6.28]	[25.6, 2, 8.52]
Solid thickness	1	1
Grid	[64, 62, 64]	[256, 193, 256]
$\boldsymbol{\Delta_y^+}$	[1, 15]	[0.49, 4.8]
$[\boldsymbol{\Delta_x^+}, \boldsymbol{\Delta_z^+}]$	[30, 15]	[14.8, 5.1]
Time step (wall-units)	0.25	0.02
Duration (wall-units)	25’000	29’000

Both the reference DNS and the present LES use long averaging time to ensure statistical convergence deep inside the solid domain. The thick solid domain used prevents the boundary condition used at the outer wall from interfering with the statistics at the fluid-solid interface.

11 passive scalars are transported by the flow. One passive scalar satisfies an imposed temperature at the fluid-wall (isoT), another satisfies an imposed heat flux at the fluid-wall (isoQ) and the 9 remaining passive scalars are subjected to fluid-solid coupling with thermal properties ratios around unity, as in Flageul et al. [2-3].

3.2. Cases at Re=7060

For the cases at Re=7060, Table II summarizes the simulation parameters.

Table II. Simulation parameters for the cases at Re=7060

	Present	**DNS**
Fluid domain extension	[6.283, 2, 3.142]	[6.283, 2, 3.142]
Solid thickness	1 (0.375)	1
Grid	[81, 106, 81]	[256, 257, 256]
$\boldsymbol{\Delta_y^+}$	[1, 15]	[0.03, 4.8]
$[\boldsymbol{\Delta_x^+}, \boldsymbol{\Delta_z^+}]$	[30, 15]	[9.6, 4.8]
Time step (wall-units)	0.22	0.016
Duration (wall-units)	220'000 (132’000)	9’500

For the first case (case 1), the solid domain is as thick as in the validation case and we have performed a DNS with the pseudo-spectral code previously used by Tiselj and Cizelj, [7]. Case 1 and the DNS contain only 3 scalars. The first satisfies an imposed temperature at the fluid-wall (isoT), the second an imposed heat flux at the fluid-wall (isoQ) and the third fluid-solid coupling with the same thermal properties in the fluid and in the solid.

For the second case (case 2), the solid domain is thinner (values between brackets in table II), thus allowing us to reduce the duration of our simulation. In wall-units, the solid domain remains thick enough so that there is no impact of the boundary condition used at the outer wall on the statistics at the fluid-solid interface. As the duration of the simulation is reduced, we can transport more scalars while keeping the computational cost of the simulations within reasonable bounds.

For case 2, 51 scalars are transported. One satisfies an imposed temperature at the fluid-wall (isoT), the second an imposed heat flux at the fluid-wall (isoQ) and the 49 others fluid-solid coupling. 7 values for the thermal diffusivity ratio and the thermal activity ratio are examined. For both parameters K and G, the same range was examined, spanning 2 decades and centered around unity: $[0.1, 0.2, 0.5, 1, 2, 5, 10]$.

4. RESULTS

4.1. Validation Results at Re=2280

LES models are designed for flows with a relatively high Reynolds number. As this validation case uses a relatively low Reynolds number, only qualitative agreement is expected.

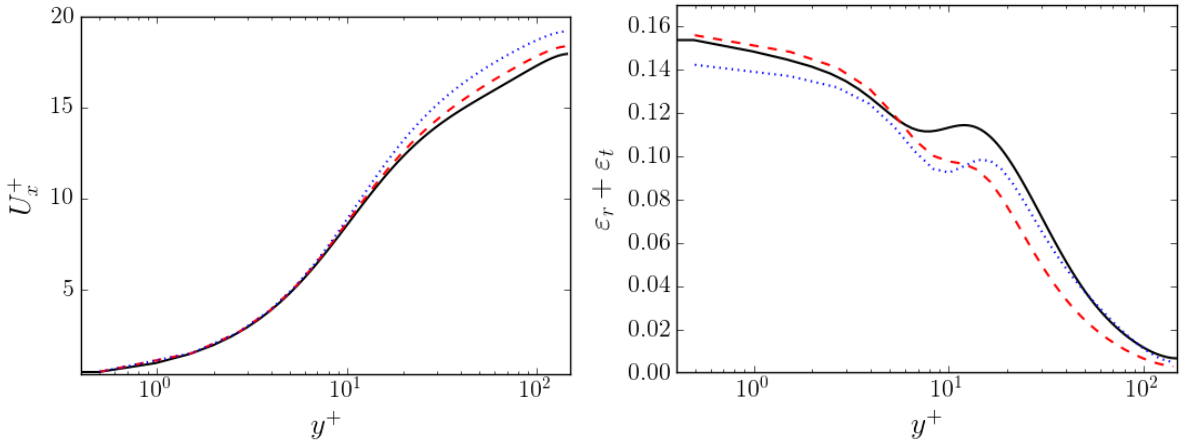

Figure 1. Left: averaged streamwise velocity. Right: estimate of the total turbulent dissipation ε. Black solid line: DNS. Red dashed line: No SGS. Blue dotted line: WALE.

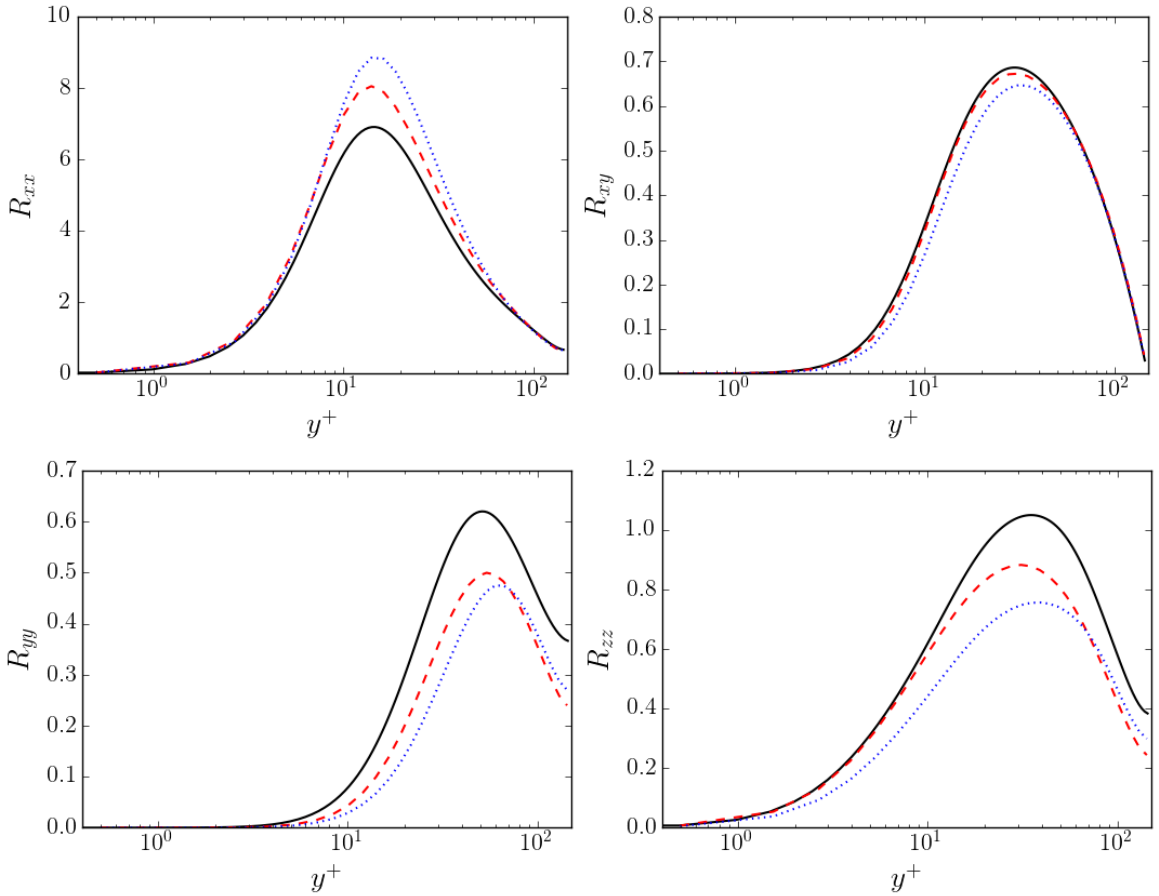

Figure 2. Reynolds stresses. Black solid line: DNS. Red dashed line: No SGS. Blue dotted line: WALE.

4.1.1. Averaged velocity, Reynolds stresses and dissipation rate ε at Re=2280

The averaged velocity and dissipation rate ε in Figure 1 show a relatively good agreement with DNS. The agreement is more qualitative for the Reynolds stresses, as shown in Figure 2.

4.1.2. Scalar-related statistics at Re=2280

As the agreement with DNS is similar for most of the scalars, only 3 are presented here: isoT, isoQ, and [G,K]=[0.5,$\sqrt{2}$]. Hereafter, the fluid (solid) domain is located at $y^+>0$ ($y^+<0$).

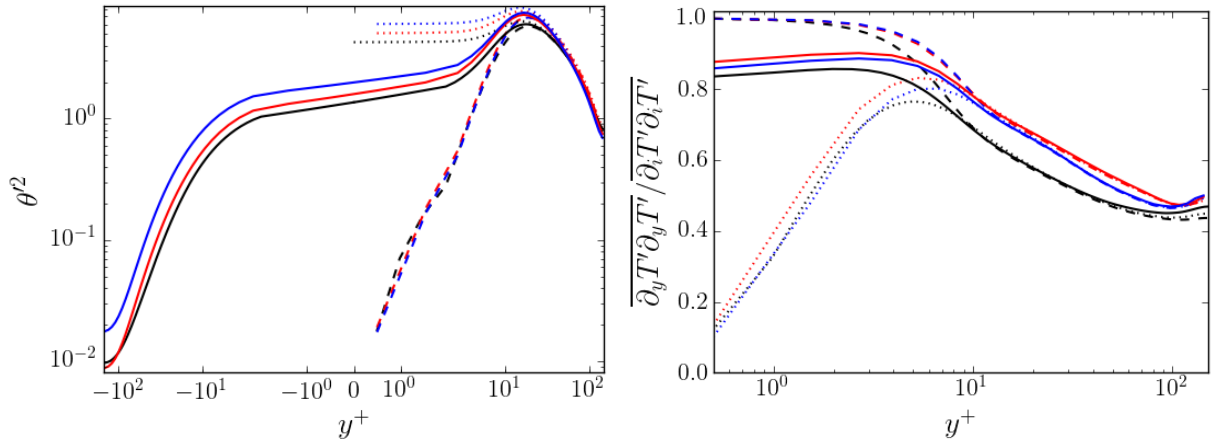

Figure 3. Left: temperature variance. Right: wall-normal contribution in $\varepsilon_{\theta,f}$. Black: DNS. Red: No SGS. Blue: WALE. Dashed lines: isoT. Dotted lines: isoQ. Solid lines: G=0.5, K=$\sqrt{2}$.

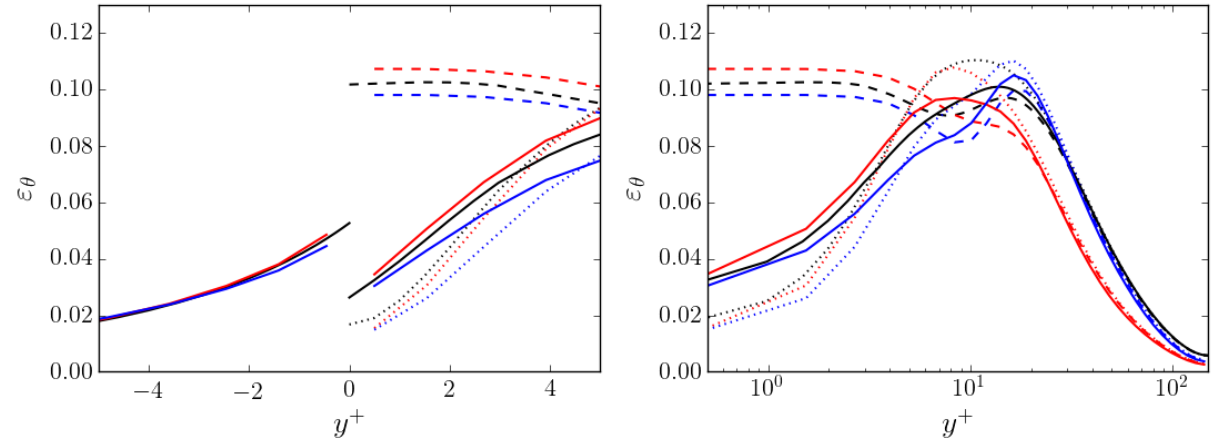

Figure 4. Left and right: ε_θ. Black: DNS. Red: No SGS. Blue: WALE. Dashed lines: isoT. Dotted lines: isoQ. Solid lines: G=0.5, K=$\sqrt{2}$.

In figure 3, the temperature variance shows a qualitative agreement with the DNS. The wall-normal contribution in ε_θ, which drives the discontinuity (following equation (8)) is slightly overestimated at the fluid-solid interface for the conjugate cases. In figure 4, the discontinuity of ε_θ at the fluid-solid interface is well estimated by the present LES, although the overall agreement in the fluid domain is only qualitative.

4.2. Case 1 at Re=7060

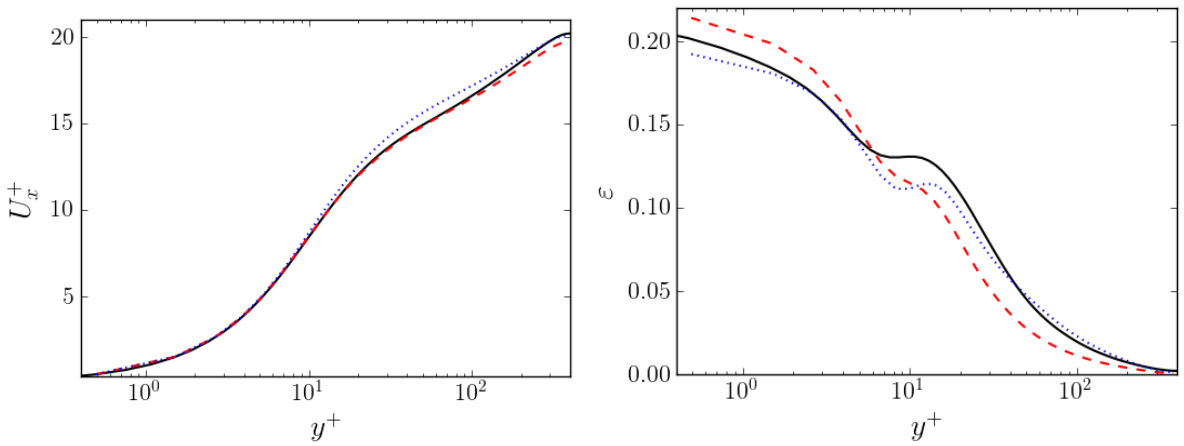

Figure 5. Left: averaged velocity. Right: ε. Black solid line: DNS. Red dashed line: No SGS. Blue dotted line: WALE.

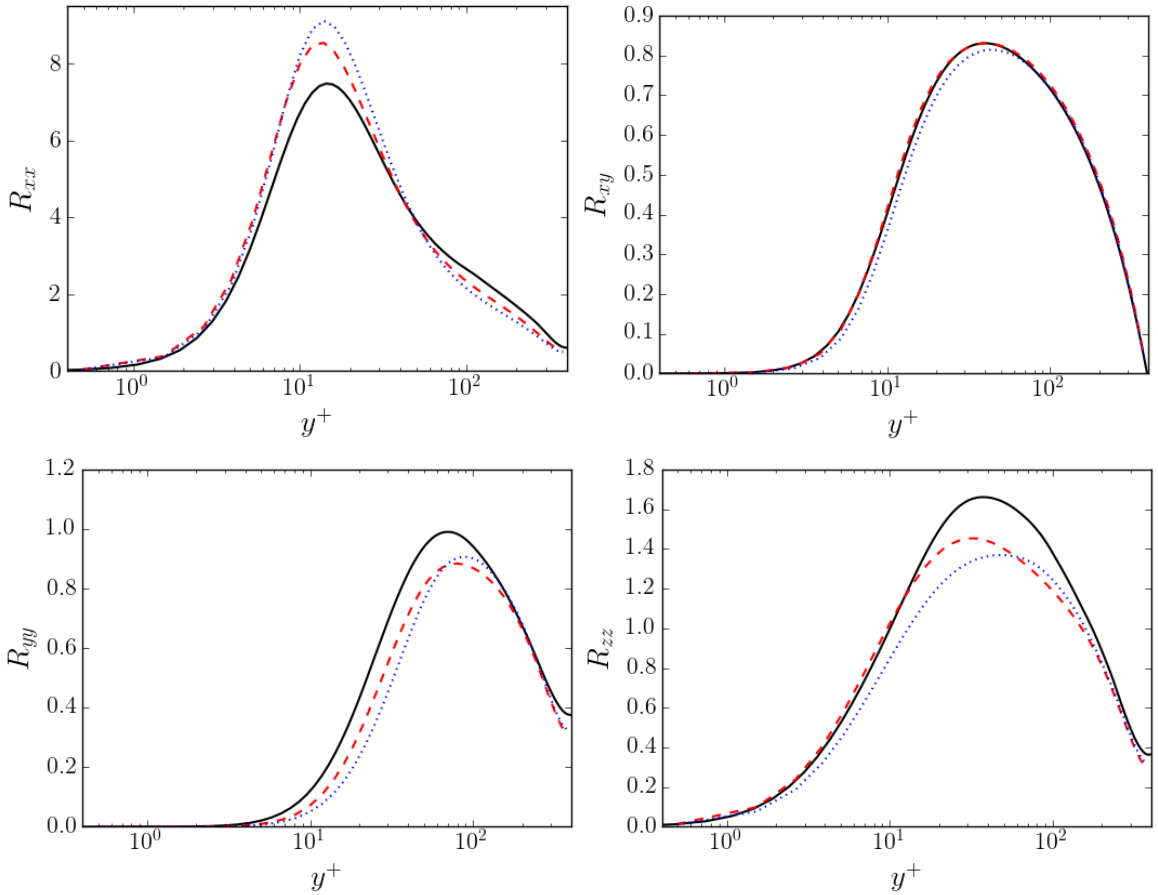

Figure 6. Reynolds stresses. Black solid line: DNS. Red dashed line: No SGS. Blue dotted line: WALE.

4.2.1. Averaged velocity, Reynolds stresses and dissipation rate ε, case 1 at Re=7060

The averaged velocity and dissipation rate ε in Figure 5 show a relatively good agreement with DNS. The agreement is still qualitative for the Reynolds stresses, as shown in Figure 6. Overall and as expected, LES performed at Re=7060 are closer to DNS, compared with the validation case at Re=2280.

4.2.2. Scalar-related statistics, case 1 at Re=7060

In figure 7, the temperature variance shows a qualitative agreement with the DNS. Our LES compare favorably with the DNS in the solid domain and at the fluid-solid interface. For the dissipation rates ε_θ plotted Figure 8, our LES results show reasonable agreement with the DNS data, especially at the fluid-solid interface where the WALE model outperforms the simulation without SGS model. For the relative wall-normal contribution in ε_θ, Figure 9 suggests that our LES overestimate it at the fluid-solid interface for conjugate cases, as observed at a lower Reynolds number (Figure 3).

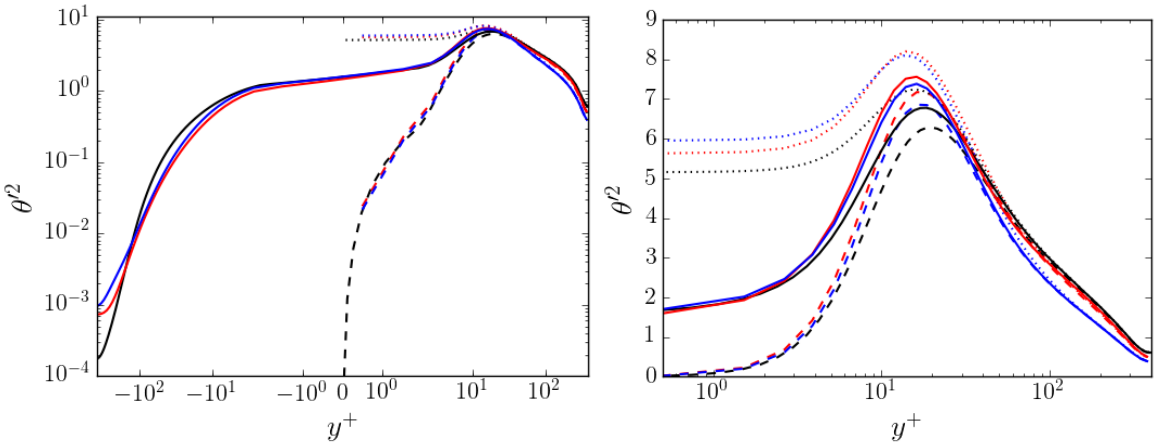

Figure 7. Left and right: temperature variance. Black: DNS. Red: No SGS. Blue: WALE. Dashed lines: isoT. Dotted lines: isoQ. Solid lines: G=1, K=1.

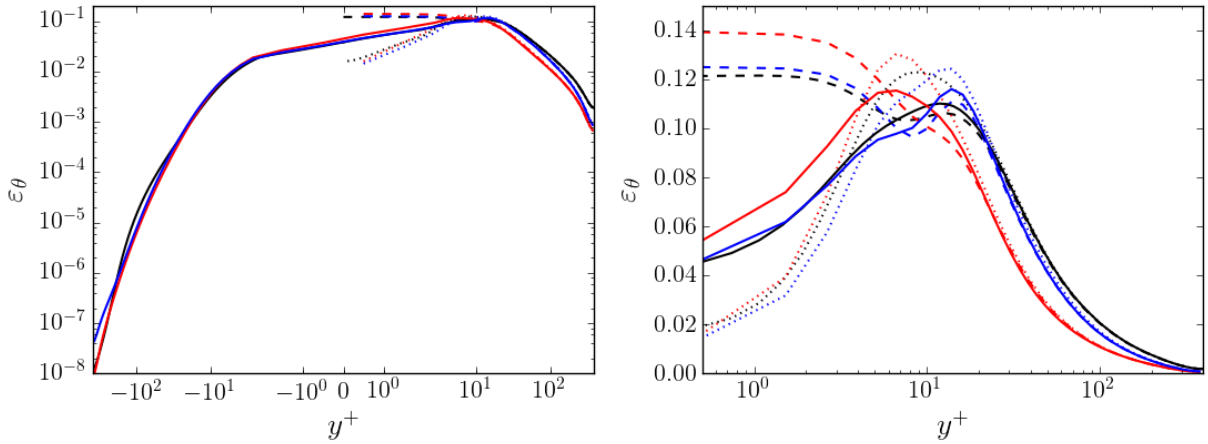

Figure 8. Left and right: ε_θ. Black: DNS. Red: No SGS. Blue: WALE. Dashed lines: isoT. Dotted lines: isoQ. Solid lines: G=1, K=1.

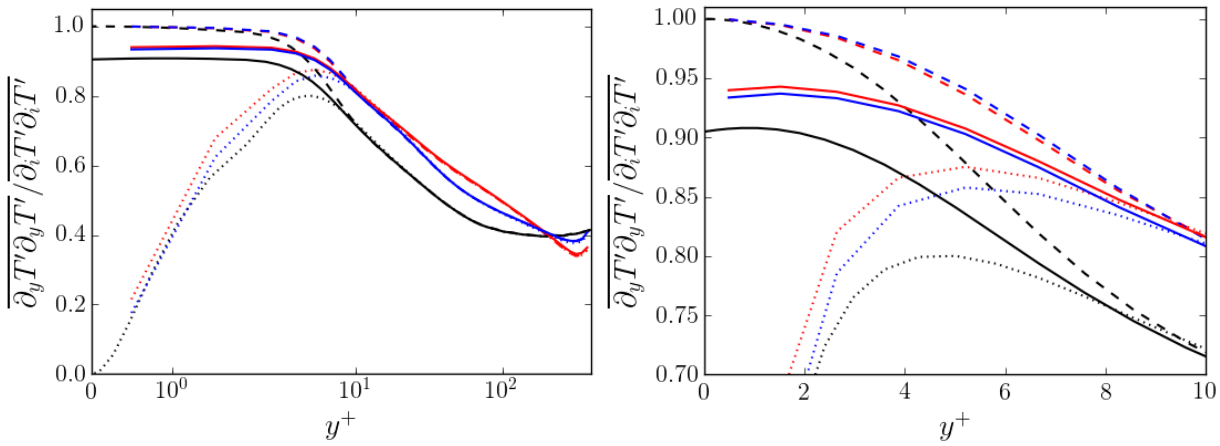

Figure 9. Left and right: wall-normal contribution in $\varepsilon_{\theta,f}$. Black: DNS. Red: No SGS. Blue: WALE. Dashed lines: isoT. Dotted lines: isoQ. Solid lines: G=1, K=1.

4.3. Case 2 at Re=7060

For case 2, average velocity, Reynolds stresses and dissipation rate ε are not plotted as they are similar to the ones in case 1.

4.3.1. Scalar-related statistics, case 2 at Re=7060

Due to the very large number of scalars transported, only partial results supporting the main conclusions are presented here. Figure 10 shows that in the fluid domain, the variance of the temperature depends mostly on the thermal activity ratio K. It is similar for the dissipation rate, which has a more complex behavior in the solid domain (Figure 11), which clearly shows the discontinuity of ε_θ. This discontinuity is driven by the relative wall-normal contribution in ε_θ, plotted in Figure 12.

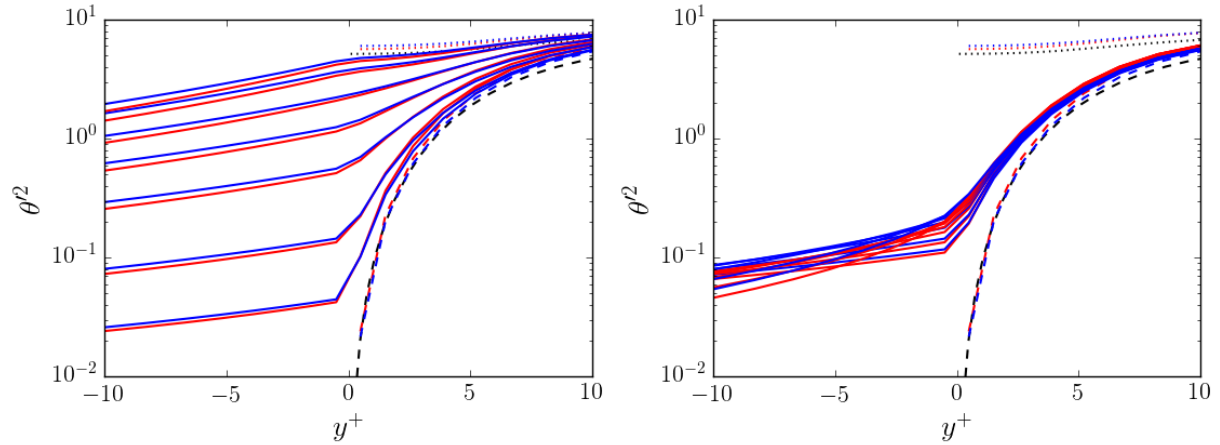

Figure 10. Left and right: temperature variance. Left: G=0.2. Right: K=0.2. Black: DNS. Red: No SGS. Blue: WALE. Dashed lines: isoT. Dotted lines: isoQ. Solid lines: Conjugate cases.

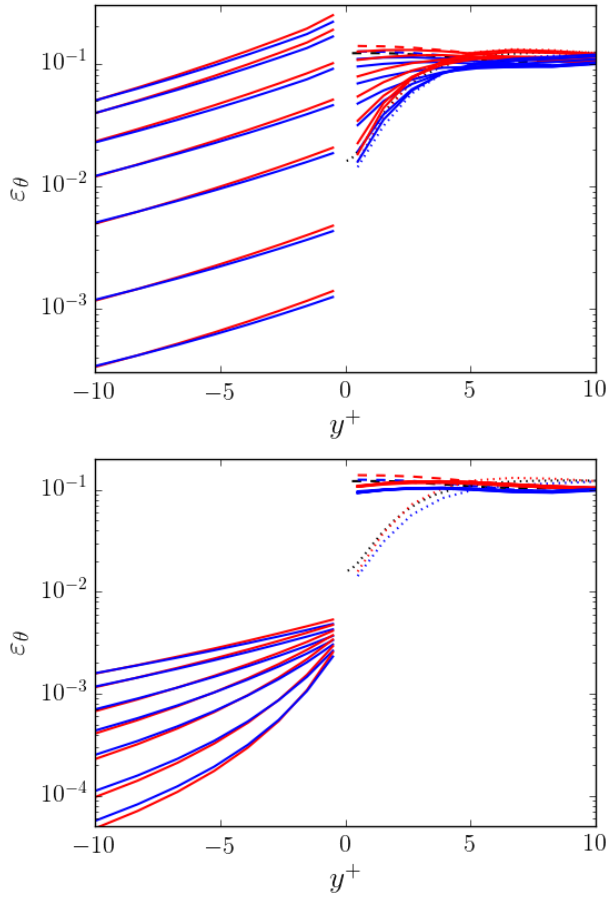

Figure 11. ε_θ. Left: G=0.2. Right: K=0.2. Black: DNS. Red: No SGS. Blue: WALE. Dashed lines: isoT. Dotted lines: isoQ. Solid lines: Conjugate cases.

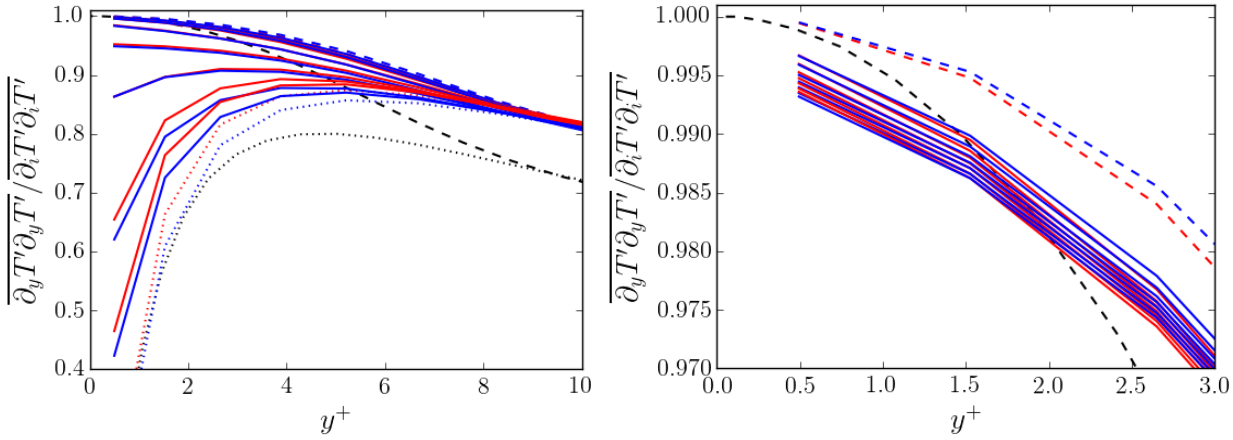

Figure 12. Wall-normal contribution in $\varepsilon_{\theta,f}$. Left: G=0.2. Right: K=0.2. Black: DNS. Red: No SGS. Blue: WALE. Dashed lines: isoT. Dotted lines: isoQ. Solid lines: Conjugate cases.

5. DISCUSSION

Qualitatively, the results show that our wall-resolved LES can quantify the discontinuity of ε_θ at the fluid-solid interface. Using equations (8) and (10), the error in our statistics can be evaluated. However, our statistics are defined at the cell center. As a result, we have no direct access to the quantities present in equation (8) as the fluid-solid interface is located at faces of cells. Fortunately, our LES are wall-resolved, so those quantities can be reconstructed with a relatively small error (first order in space). First, we recall equation (8) and reorder it to use the relative wall-normal contribution in the solid domain:

$$\frac{\varepsilon_{\theta,s}}{\varepsilon_{\theta,f}} = \frac{\overline{\partial_n T_f' \partial_n T_f'}}{\overline{\partial_\iota T_f' \partial_\iota T_f'}} K^2 + \left(1 - \frac{\overline{\partial_n T_f' \partial_n T_f'}}{\overline{\partial_\iota T_f' \partial_\iota T_f'}}\right) \frac{1}{G} \text{ at } \partial\Omega_f \cap \partial\Omega_s. \tag{12}$$

$$\frac{\varepsilon_{\theta,f}}{\varepsilon_{\theta,s}} = \frac{\overline{\partial_n T_s' \partial_n T_s'}}{\overline{\partial_\iota T_s' \partial_\iota T_s'}} \frac{1}{K^2} + \left(1 - \frac{\overline{\partial_n T_s' \partial_n T_s'}}{\overline{\partial_\iota T_s' \partial_\iota T_s'}}\right) G \text{ at } \partial\Omega_f \cap \partial\Omega_s. \tag{13}$$

However, following figure 12, one may say that the relative wall-normal contribution at $y^+=\pm 0.5$ is only a crude approximation of the relative wall-normal contribution at the fluid-solid interface. Using Taylor expansion, the variance of the temperature at the fluid-solid interface can be reconstructed more accurately. We reconstruct it with a quadratic Taylor expansion. We also reconstruct the relative wall-normal contribution at the fluid-solid interface using a linear Taylor expansion. This is further described in appendix A. Table III gives the value of the square root of the product of equations (12) and (13) for the WALE simulation. Results are similar for the simulation without SGS model.

Table III. Geometrical mean of the reconstructed dissipation ratios in equations (12) and (13), case 2, WALE simulation. Theoretical value is 1.

	K=0.1	**K=0.2**	**K=0.5**	**K=1**	**K=2**	**K=5**	**K=10**
G=0.1	1.002	1.005	1.011	1.018	1.022	1.015	1.000
G=0.2	1.001	1.003	1.007	1.010	1.010	1.000	0.984
G=0.5	1.000	1.000	1.001	1.001	1.000	0.995	0.991
G=1	0.999	0.999	0.999	1.000	1.002	1.009	1.022
G=2	0.999	0.999	1.000	1.004	1.012	1.039	1.079
G=5	0.999	1.000	1.005	1.015	1.039	**1.108**	**1.206**
G=10	1.000	1.002	1.011	1.030	1.073	**1.193**	**1.363**

Values written in a bold font and underlined indicate an error above 10%. For most of the scalars considered here, the combination of the statistical error and the reconstruction approximation is limited to a few percent, or less. However, cases with a high K and a high G give rise to higher errors. The source of this higher error is currently unknown. High values of G are associated with large time scales for the temperature fluctuations in the solid domain. Therefore, the present results at high G and K may be biased by statistical convergence and need deeper analysis.

At the fluid-solid interface, θ'^2 is less than 10% of the isoQ value for all the conjugate cases with $K \leq 0.2$, and for the cases with K=0.5 and $G \leq 0.2$. From this perspective, the present conjugate cases quickly converge towards the isoT case for thermal activity ratios below unity. The maximal value of θ'^2 is around 84% of the isoQ one and is obtained with K=10 and G=10. One may conclude that the thermal properties ratios studied here are not far enough from unity to reach the isoQ case. However, as already stated, the present results at high G and K may be biased by statistical convergence and need deeper analysis.

The present simulations resulted in a relatively huge dataset. The authors are currently analyzing it. Our main objective is to extract scaling laws from the statistics related to the coupled scalars at the fluid-solid interface and in the solid domain, with the hope that those scaling laws will be useful for future (U)RANS turbulence models and LES wall-models.

6. CONCLUSIONS

The results presented here show that wall-resolved LES can be used to quantify the discontinuity of ε_θ at the fluid-solid interface in case of conjugate heat transfer. The combination of the WALE SGS model and a constant turbulent Prandtl number of 0.5 showed good agreement with available DNS results. Using equations (12) and (13), we also propose an indicator allowing one to evaluate the error at the fluid-solid interface. This indicator is useful as it is stand-alone and derived solely from the continuity of temperature and heat flux at the fluid-solid interface.

From the perspective of a rich validation database for future (U)RANS models for conjugate heat transfer adapted to the discontinuity of ε_θ, this is encouraging as more complex configurations, closer to industrial applications, can be investigated on the basis of the present work, which uses a relatively simple SGS model. The proposed error indicator will give an objective criterion to assess the accuracy of the statistics in the aforementioned future database.

However, much more work remains necessary to confidently assess industrial challenges. Aside from more complex geometries, an interesting perspective is the extension towards active scalar cases for which the fluid-solid coupling can potentially change the whole flow and heat transfer. This will require a careful examination to make sure the present SGS model handles correctly buoyancy effects or variable fluid properties, such as the ones encountered in supercritical applications.

ACKNOWLEDGMENTS

The authors thank EDF R&D and the institute Jožef Stefan for funding the present study and providing computational time.

REFERENCES

1. T.J. Craft, H. Iacovides and S. Uapipatanakul, “Towards the development of RANS models for conjugate heat transfer,” *Journal of turbulence*, **11**, (2010).
2. C. Flageul, S. Benhamadouche, E. Lamballais and D. Laurence, "DNS of turbulent channel flow with conjugate heat transfer: Effect of thermal boundary conditions on the second moments and budgets", *International Journal of Heat and Fluid Flow*, **55**, (2015).
3. C. Flageul, S. Benhamadouche, E. Lamballais and D. Laurence, “On the discontinuity of the dissipation rate associated with the temperature variance at the fluid-solid interface for cases with conjugate heat transfer”, *International Journal of Heat and Mass Transfer*, **Submitted**, (2017).
4. F. Nicoud, and F. Ducros, “Subgrid-scale stress modelling based on the square of the velocity gradient tensor,” *Flow, turbulence and combustion*, **62**, (1999).
5. G. Grötzbach, "Revisiting the resolution requirements for turbulence simulations in nuclear heat transfer", *Nuclear Engineering and Design*, **241**, (2011).
6. N. Kasagi, Y. Tomita and A. Kuroda, “Direct numerical simulation of passive scalar field in a turbulent channel flow,” *Journal of Heat Transfer,* **114**, (1992).
7. I. Tiselj and L. Cizelj, “DNS of turbulent channel flow with conjugate heat transfer at Prandtl number 0.01,” *Nuclear Engineering and Design*, **253**, (2012).

8. F. Archambeau, N. Mechitoua and M. Sakiz, "*Code_Saturne*: a finite volume code for the computation of turbulent incompressible flows – industrial applications", *International Journal on Finite Volumes*, **1**, (2004).

APPENDIX A

In the first cell, both in the fluid and in the solid domain, we approximate the variance of the temperature with a quadratic Taylor expansion:

$$T'^2_f(y) = \theta'^2_f + a_f(y - y_f) + b_f(y - y_f)^2 \text{ in the first fluid cell.} \quad (14a)$$
$$T'^2_s(y) = \theta'^2_s + a_s(y - y_s) + b_s(y - y_s)^2 \text{ in the first solid cell.} \quad (14b)$$

The center of the first cells are located at y_f and y_s while the fluid-solid interface is located at y_{fs}. The variance of the temperature at the cell centers (θ'^2_f and θ'^2_s) is known. We assume the flow is statistically steady. In addition, in the first cell, we assume equilibrium of dissipation and molecular diffusion in the budget equation of θ'^2_f, which is reasonable for a wall-resolved LES. This leads to

$$b_f = Pr\varepsilon_{\theta,f} \text{ and } b_s = Pr\varepsilon_{\theta,s} \quad (15)$$

As the dissipation rates at the cell centers are known, 2 unknown remains. They are derived from the continuity of temperature and heat flux:

$$T'^2_f(y_{fs}) = T'^2_s(y_{fs}) \text{ and } \lambda_f \partial_y T'^2_f(y_{fs}) = \lambda_s \partial_y T'^2_s(y_{fs}). \quad (16)$$

The ratio of thermal conductivities can be derived from the thermal properties ratios:

$$\frac{\lambda_s}{\lambda_f} = G_2 = \frac{1}{K\sqrt{G}}. \quad (17)$$

The resulting 2x2 system is:

$$\begin{pmatrix} 1 & -G_2 \\ -(y_{fs} - y_f) & y_{fs} - y_s \end{pmatrix} \begin{pmatrix} a_f \\ a_s \end{pmatrix} = \begin{pmatrix} -2Pr\varepsilon_{\theta,f}(y_{fs} - y_f) + 2G_2 Pr\varepsilon_{\theta,s}(y_{fs} - y_s) \\ \theta'^2_f + Pr\varepsilon_{\theta,f}(y_{fs} - y_f)^2 - \theta'^2_s - Pr\varepsilon_{\theta,s}(y_{fs} - y_s)^2 \end{pmatrix}. \quad (18)$$

We have injected the solution in equation (14a) to compute $T'^2_f(y_{fs})$.

The terms $\overline{\partial_x T' \partial_x T'}$ and $\overline{\partial_z T' \partial_z T'}$ are treated similarly using a linear Taylor expansion, their continuity at the fluid-solid interface and the discontinuity of their wall-normal derivative, which behaves like the derivative of the temperature variance at the fluid-solid interface.

At the fluid-solid interface, the term $\overline{\partial_y T' \partial_y T'}$ is also discontinuous:

$$\lambda_f{}^2 . \partial_y T'_f . \partial_y T'_f(y_{fs}) = \lambda_s{}^2 . \partial_y T'_s . \partial_y T'_s(y_{fs}). \quad (19)$$

However, for this last quantity, no compatibility condition involving its derivative is available so we don't use a linear Taylor expansion. We use the normalized one-point correlation associated with the temperature and its wall-normal derivative, which is continuous at the fluid-solid interface:

$$\frac{\overline{T'_f \partial_y T'_f}}{\sqrt{\overline{T'_f}^2}\sqrt{\overline{\partial_y T'_f \partial_y T'_f}}} = \frac{\overline{T'_s \partial_y T'_s}}{\sqrt{\overline{T'_s}^2}\sqrt{\overline{\partial_y T'_s \partial_y T'_s}}} \text{ at the fluid-solid interface.} \quad (20)$$

On both sides of equation (20), the numerator is the halved derivative of the temperature variance. This quantity and the root mean square of the temperature are available at the fluid-solid interface using equations (14a) and (14b). In addition, we assume that this normalized correlation at the fluid-solid interface is the arithmetic mean of the corresponding values at the first fluid and solid cell center. This strategy allows us to reconstruct the relative wall-normal contribution at the fluid-solid interface.